



HAL
open science

A model problem for the evolution of strain structure at the crossing of a flame front

Michel Gonzalez

► **To cite this version:**

Michel Gonzalez. A model problem for the evolution of strain structure at the crossing of a flame front. *Theoretical and Computational Fluid Dynamics*, 2022, 36 (4), pp.627-639. 10.1007/s00162-022-00618-x . hal-03754142

HAL Id: hal-03754142

<https://hal.science/hal-03754142>

Submitted on 14 Oct 2022

HAL is a multi-disciplinary open access archive for the deposit and dissemination of scientific research documents, whether they are published or not. The documents may come from teaching and research institutions in France or abroad, or from public or private research centers.

L'archive ouverte pluridisciplinaire **HAL**, est destinée au dépôt et à la diffusion de documents scientifiques de niveau recherche, publiés ou non, émanant des établissements d'enseignement et de recherche français ou étrangers, des laboratoires publics ou privés.

A model problem for the evolution of strain structure at the crossing of a flame front

M. Gonzalez

Received: date / Accepted: date

Abstract The local thermal effect of a flame front is simulated by a model for a mass density front by specifying a likely expansion rate. This model problem includes two independent parameters, namely the heat release parameter and a parameter akin to a Karlovitz number. The analysis is focused on the influence of the Karlovitz number on the evolution of strain properties at the crossing of the front. The latter are derived from an equation system for the velocity gradient tensor and the pressure Hessian tensor undergoing the forcing of the expansion rate. Strain eigenvalues, orientation of strain principal axes, and stretching in the direction of forcing are especially scrutinized. Furthermore, the model shows that, when approaching a flame front, the special alignments of strain are mostly caused by anisotropy of pressure Hessian resulting from forcing by expansion.

Keywords Velocity gradient · Strain structure · Premixed flames · Variable mass density · Pressure Hessian

1 Introduction

Micromixing is the mere expression of the small-scale action of flow on scalar fields, more precisely, the outcome of the mechanical action exerted by the velocity gradient on the gradients of scalars. The straining part of the velocity gradient, at least in incompressible flows, tends to enhance scalar gradients through compression, thereby hastening local diffusive fluxes. Thus the level of micromixing tightly depends on strain main properties, namely intensity, direction, and lifetime.

Mixing in non-solenoidal flows is a special case, for mass density variations may deeply affect the velocity gradient. Alteration of the intensity and/or orientation of strain, then, may influence the micromixing process. This is especially relevant in compressible flows [1,2] and in reacting flows with heat release such as flames [3–9]. More specifically, scalar dissipation – the key mechanism driving

M. Gonzalez
CNRS, UMR 6614/CORIA, Site universitaire du Madrillet
76801 Saint-Etienne du Rouvray, France
E-mail: michel.gonzalez@coria.fr

micromixing – may be altered through the mechanism of stretching [4, 10, 11]. Understanding those phenomena therefore definitely needs addressing the influence of local mass density variations on strain structure. In particular, the evolution of strain undergoing local heat release was addressed in premixed flames, which showed that principal strain levels as well as strain axes orientation were affected [8, 12–14].

The latter works considered the full, intricate interaction between the velocity gradient and reacting scalar gradients. The present study, by contrast, refers to a step-by-step approach in which the basic underlying mechanisms are analyzed separately. In this regard, a model problem was already proposed and was shown to reliably simulate strain features observed in premixed flame fronts through the heat release parameter [15]. The model is now supplemented with an additional parameter akin to a Karlovitz number, and the analysis addresses the changes of strain structure when this Karlovitz number is varied. A major aspect of this work is to focus analysis on the role of pressure Hessian in the behavior of strain at the crossing of the front. Mechanisms involving the pressure Hessian were already suggested by previous works [18, 22] and recently addressed in model and numerical simulation [8, 15].

The model problem described in Section 2 is based on two main principles. First, the expansion rate is specified in function of a progress variable to mimic mass density variation at the crossing of a flame front. And second, the dynamic field, defined by the velocity gradient tensor and the pressure Hessian tensor, is forced by the expansion rate through one diagonal component of the pressure Hessian. The resulting forcing direction may refer to the normal to a flame front. The equation system for the velocity gradient tensor is closed with the enhanced homogenized Euler equation (EHEE) model of Suman and Girimaji [16] and is solved in a two-dimensional Euler flow.

In Section 3, the structure of strain undergoing the effect of expansion rate is scrutinized through the evolution of strain eigenvalues and strain axes orientation. The role of pressure Hessian in the rotation of strain principal axes is especially emphasized. In addition, the influence of Karlovitz number on stretching parallel to the direction of forcing – an issue specifically relevant to flame problems – is discussed. Finally, the influence of initial conditions is checked.

2 Model problem

In an Euler flow, the evolution of the velocity gradient tensor, $\mathbf{A} = \nabla \mathbf{u}$, is described by the following equation:

$$\frac{DA_{ij}}{Dt} = -A_{i\alpha}A_{\alpha j} - \Pi_{ij}, \quad (1)$$

where the Π_{ij} 's are the components of the pressure Hessian tensor, $\Pi = \nabla[(\nabla p)/\rho]$, with p and ρ being respectively the pressure and the mass density.

In the two-dimensional case, Eq. (1) can be expressed by a four-equation system:

$$\frac{D\sigma_n}{Dt} = -\delta\sigma_n + \Pi_{22} - \Pi_{11}, \quad (2)$$

$$\frac{D\sigma_s}{Dt} = -\delta\sigma_s - \Pi_{12} - \Pi_{21}, \quad (3)$$

$$\frac{D\omega}{Dt} = -\delta\omega + \Pi_{12} - \Pi_{21}, \quad (4)$$

$$\frac{DP}{Dt} = -\frac{1}{2}(\sigma^2 - \omega^2 + P^2) - \Pi_{11} - \Pi_{22}, \quad (5)$$

where $\delta(t)$ is the expansion – or dilatation – rate, $\delta(t) = -1/\rho \cdot D\rho/Dt$, $\sigma_n = A_{11} - A_{22}$ and $\sigma_s = A_{12} + A_{21}$ are, respectively, the normal and shear components of strain, $\sigma = (\sigma_n^2 + \sigma_s^2)^{1/2}$ is the strain intensity, $\omega = A_{21} - A_{12}$ is the vorticity, and $P = A_{11} + A_{22}$ is the velocity divergence, $\nabla \cdot \mathbf{u}$. As a result of mass conservation, P coincides with the expansion rate: $P \equiv \delta$; in the following, notation P is dropped.

Consistently with the progress variable used in premixed flame problems, a nondimensional variable, $c(t)$, is defined as $c(t) = (\rho_o/\rho(t) - 1)/(\rho_o/\rho_\infty - 1)$ where $\rho_o \equiv \rho(0)$, and $\rho_\infty \equiv \lim_{t \rightarrow \infty} \rho(t)$; the density ratio is defined by ρ_o/ρ_∞ . From the definitions of $c(t)$ and $\delta(t)$:

$$\frac{Dc}{Dt} = \left(c + \frac{1}{q}\right) \delta, \quad (6)$$

with $q = \rho_o/\rho_\infty - 1$. In this study, $\rho_\infty < \rho_o$, which means $q > 0$, and $\delta > 0$ as a result of heat release.

As a first feature, the model problem mimics the expansion rate at the crossing of a flame front by assuming δ as:

$$\delta(c) = 4\delta_m c(1 - c), \quad (7)$$

where δ_m is the maximum value of $\delta(c)$. The parabolic function modelling $\delta(c)$ is inspired from numerical simulation data for the velocity divergence across a flame front [12]. Note that from the approach of Tien and Matalon [17] $\delta \simeq q/\tau_f$ in the reaction zone of a premixed flame, where τ_f is the flame timescale. Consequently, δ_m is taken as: $\delta_m \simeq q/\tau_f$. The problem is made nondimensional by using some reference strain intensity, σ_0 , which does not change the form of the above equations. And the nondimensional δ_m is q/Ka_0 , where $Ka_0 = \tau_f \sigma_0$ can be seen as a Karlovitz number. Throughout the manuscript, the initial notation is kept for variables made nondimensional with σ_0 . Equation (6) can then be written as:

$$\frac{Dc}{Dt} = 4\frac{q}{Ka_0} \left(c + \frac{1}{q}\right) c(1 - c). \quad (8)$$

This model problem thus includes two independent parameters, namely the heat release parameter, q , and the ratio of expansion timescale to strain timescale, Ka_0 . Figure 1 shows $\delta(t)$ for $q = 5$ and $Ka_0 = 0.5, 1., 2.,$ and 4 . In an Eulerian view, the Lagrangian evolution of the expansion rate displayed in Fig. 1 comes to the crossing of a restricted spatial region in which the expansion rate is prescribed to mimic a flame front.

Now, as the velocity divergence is prescribed through the expansion rate, δ , Eq. (5) is not needed to determine the velocity tensor. The second feature of the model, then, consists in using Eq. (5) to compute one diagonal component of the pressure Hessian, say, Π_{11} , as:

$$\Pi_{11} = -\Pi_{22} - \frac{1}{2}(\sigma^2 - \omega^2) - \frac{1}{2} \left(\delta^2 + 2\frac{D\delta}{Dt} \right). \quad (9)$$

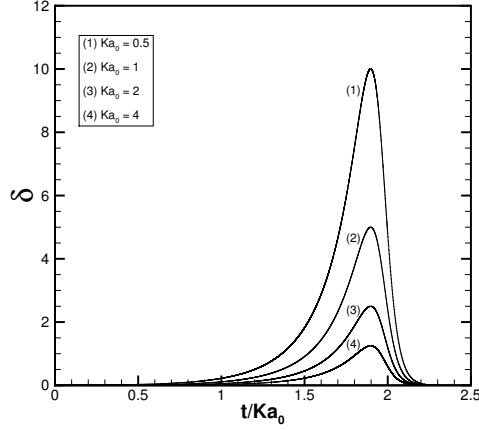


Fig. 1 Evolution of expansion rate, $\delta(t)$, for heat release parameter $q = 5$ and Karlovitz number $Ka_0 = 0.5, 1, 2,$ and 4 . The peak in the expansion rate increases as the Karlovitz number decreases

This comes to define a special direction $-x_1$, in the present case – along which the forcing resulting from the expansion rate takes place.

The other components of the pressure Hessian, namely Π_{12} , Π_{21} , and Π_{22} , are computed using the EHEE modelled equation [16]:

$$\frac{D\Pi_{ij}}{Dt} = -A_{\alpha j}\Pi_{i\alpha} - A_{\alpha i}\Pi_{\alpha j} - (n-1)A_{\alpha\alpha}\Pi_{ij}, \quad (10)$$

in which n is the ratio of specific heats. In a sense, the present approach models the pressure Hessian with a ‘forced EHEE model’. With the above specific, two-dimensional notation, Eq. (10) leads to:

$$\frac{D\Pi_{12}}{Dt} = -n\delta\Pi_{12} - \frac{1}{2}(\sigma_s - \omega)\Pi_{11} - \frac{1}{2}(\sigma_s + \omega)\Pi_{22}, \quad (11)$$

$$\frac{D\Pi_{21}}{Dt} = -n\delta\Pi_{21} - \frac{1}{2}(\sigma_s - \omega)\Pi_{11} - \frac{1}{2}(\sigma_s + \omega)\Pi_{22}, \quad (12)$$

$$\frac{D\Pi_{22}}{Dt} = (-n\delta + \sigma_n)\Pi_{22} - \frac{1}{2}(\sigma_s - \omega)(\Pi_{12} + \Pi_{21}). \quad (13)$$

Finally, running the model needs solving Eqs. (2) - (4), Eq. (8), and Eqs. (11) - (13), together with Eq. (7) for δ , and Eq. (9) for Π_{11} , with relevant initial conditions. The solution method uses an explicit-in-time numerical scheme. In the present work, only initial conditions for normal strain and vorticity, namely $\sigma_n(0)$ and $\omega(0)$, are varied (Section 3); the other initial conditions are: $c(0) = 10^{-4}$, $\sigma_s(0) = 0$, and initial isotropy of pressure Hessian, namely $\Pi_{12}(0) = \Pi_{21}(0) = 0$, and $\Pi_{11}(0)$ and $\Pi_{22}(0)$ derived from Eq. (5) at $t = 0$, with $\Pi_{11}(0) = \Pi_{22}(0)$, i.e.:

$$\Pi_{11}(0) = \Pi_{22}(0) = -\frac{1}{4}[\sigma(0)^2 - \omega(0)^2] - \frac{1}{4}\left[\delta(0)^2 + 2\frac{D\delta}{Dt}\Big|_{t=0}\right]. \quad (14)$$

Note that production of Π_{12} and Π_{21} is triggered by the interaction between ω and the diagonal components of pressure Hessian, Π_{11} and Π_{22} – Eqs. (11) and (12) –, and that σ_s is in turn produced by Π_{12} and Π_{21} – Eq. (3).

3 Effect of Karlovitz number on strain structure

3.1 Reference test case

An earlier study addressed the effect of heat release for $Ka_0 = 1$ [15]. The results reported in this section were derived for $q = 5$ and $Ka_0 = 0.5, 1., 2.,$ and $4.$ In addition, $\sigma_n(0) = -Ka_0\delta_m$ – which ensures that $\sigma_n(0)$ does not change with Ka_0 –, and $\omega(0) = \sigma(0)$; the influence of those initial conditions is discussed in next section.

The nondimensional ratio of expansion rate to local strain intensity, δ/σ , is a critical parameter of the problem. Values of δ/σ exceeding unity indicate that heat release prevails over flow strain, and imply that the lowest strain eigenvalue is positive, in other words, that both directions of strain are extensional [18]; strain has one compressional direction if $\delta/\sigma < 1$. Note that this ratio can be considered as the reciprocal local Karlovitz number, Ka . The influence of Ka_0 upon δ/σ is shown in Fig. 2. Ratio δ/σ is greater than one over a significant range of c values, meaning fully extensional strain thereover, except for the greatest value of Ka_0 . This special feature certainly stems from the two-dimensional nature of the problem. Fully extensional strain seems to be less likely in three-dimensional flames even if positive values of lowest strain has been observed in some studies [4, 19]. As Ka_0 is decreased, the c -range affected by prevailing expansion widens; the peaks showing highest dominance of expansion over strain are pushed towards the lower and upper ends where variation of δ/σ also gets stiffer.

Figure 3 shows the strain eigenvalues made nondimensional using the flame timescale, τ_f , that is, $\lambda_i^* = Ka_0 \cdot \lambda_i$, with $\lambda_1 = (-\sigma + \delta)/2$ and $\lambda_2 = (\sigma + \delta)/2$ being respectively the lowest and highest eigenvalues; $\delta^* = \lambda_1^* + \lambda_2^* = Ka_0 \cdot \delta$ does not depend on the Karlovitz number. As expected, λ_1^* is hardly positive for $Ka_0 = 4$, and gets positive over a wider c -range as Ka_0 is decreased. For $Ka_0 = 0.5$, the model approaches the special case of the free plane premixed flame for which – as it is easy to show – λ_1 vanishes and strain is merely extensional. Although their work is on turbulent three-dimensional flames, Kasten *et al.* [14] recently observed a similar behavior of the mean strain eigenvalues when varying the Karlovitz number (Fig. 4).

The other essential strain feature is the orientation of principal axes. Angle $\Phi = \arctan(\sigma_n/\sigma_s)/2 - \pi/4$ indicates orientation of highest strain direction, \mathbf{e}_2 , with respect to forcing direction, \mathbf{x}_1 . It is plotted in Fig. 5 for $Ka_0 = 0.5, 1, 2,$ and $4.$ For $Ka_0 = 2,$ and $4,$ $\Phi < -\pi/4$ – which means that direction \mathbf{x}_1 feels the action of lowest strain – throughout c -range. For $Ka_0 = 0.5,$ and $1,$ by contrast, $\Phi > -\pi/4$ – which means direction \mathbf{x}_1 undergoing highest strain – over a significant range. The latter clearly widens, and alignment of highest strain with \mathbf{x}_1 gets better, with decreasing Karlovitz number. In addition, alignment of lowest strain with \mathbf{x}_1 at the lower and upper ends of c -range, and of highest strain with \mathbf{x}_1 within the intermediate range is reminiscent of switching alignment of strain axes with the normal to a flame front as reported in previous studies [8, 14, 20]. Figure 6 shows the

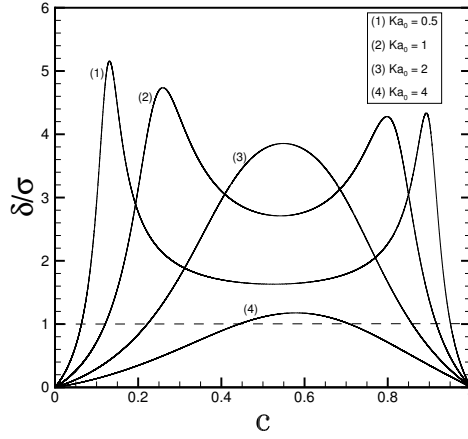


Fig. 2 Expansion rate-to-strain rate ratio, δ/σ , vs. progress variable, c , for Karlovitz number $Ka_0 = 0.5, 1, 2$, and 4 . The c -range where expansion prevails over strain widens with decreasing Karlovitz number

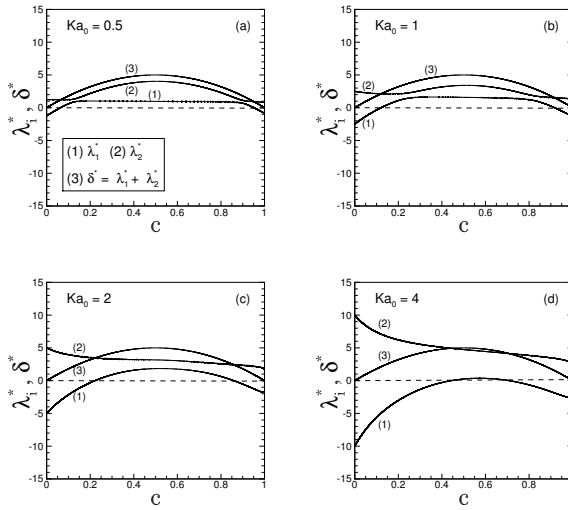


Fig. 3 Strain eigenvalues normalized by flame timescale, λ_i^* , and $\delta^* = \lambda_1^* + \lambda_2^*$, vs. progress variable, c , for Karlovitz number $Ka_0 = 0.5, 1, 2$, and 4 . The lowest strain eigenvalue, λ_1^* , gets positive over a wider c -range with decreasing Karlovitz number

orientation of strain rate principal axes with respect to the normal to the flame front computed by Kasten *et al.* [14]; as for strain eigenvalues (Figs. 3 and 4), although a point-by-point comparison would be irrelevant – the model is Lagrangian, two-dimensional, inviscid, and assumes a one-way coupling between heat release and

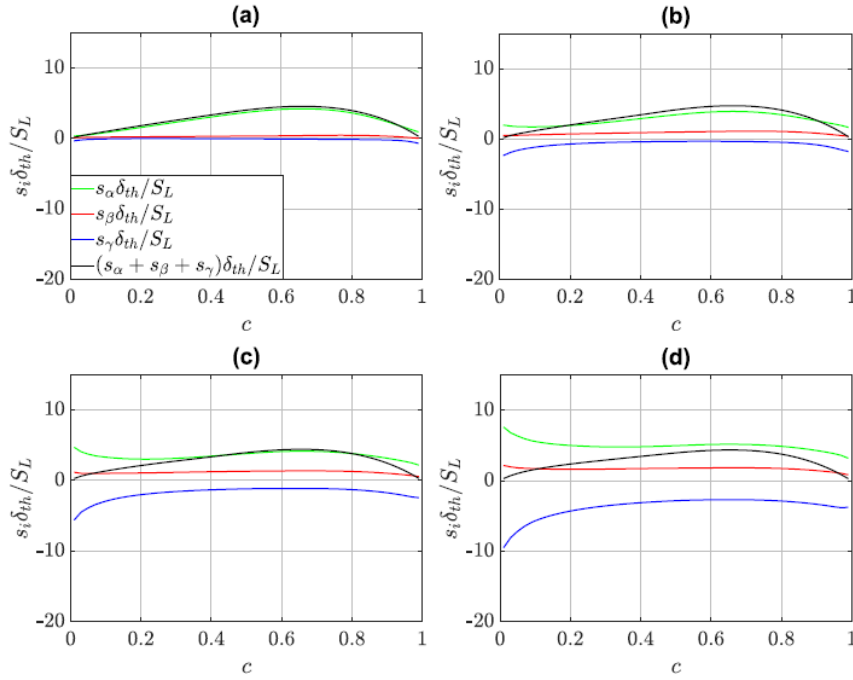


Fig. 4 Strain eigenvalues, s_α , s_β , and s_γ (with $s_\alpha > s_\beta > s_\gamma$), and dilatation rate, $s_\alpha + s_\beta + s_\gamma$, normalized by flame timescale, conditioned upon c for heat release parameter 4.5 and Karlovitz number 0.58 (a), 3 (b), 6.5 (c), and 11.9 (d) [14]. The evolution of eigenvalues λ_1^* and λ_2^* (Fig. 3) is to be compared with the evolution of above s_γ (blue line) and s_α (green line), respectively. Reproduced from “Principal strain rate evolution within turbulent premixed flames for different combustion regimes” by Kasten, C., Ahmed, U., Klein, M., Chakraborty, N., *Physics of Fluids* **33**, 015111 (2021) with permission of AIP Publishing

the velocity gradient –, evolution with Karlovitz number of the orientation of highest strain predicted by the model is clearly akin to their numerical data. As already shown, this special behavior of strain most likely results from anisotropy of the pressure Hessian promoting rotation of principal axes [15], which is analyzed further below.

Stretching along direction \mathbf{x}_1 refers to straining normal to a flame front. The latter is a key issue in flame problems [4,11], for it results in the interaction of gradients of scalars – such as the progress variable, concentrations, or temperature – with velocity gradients, thereby determining the production of scalar dissipation and thus the process of small-scale mixing. Stretching parallel to \mathbf{x}_1 depends both on strain eigenvalues and orientation of principal axes with respect to \mathbf{x}_1 , $\theta_1 = \pi/2 - \Phi$ – for lowest strain –, and $\theta_2 = \Phi$ – for highest strain. Figure 7 shows those latter contributions, $s_1^* = -\lambda_1^* \cos^2 \theta_1$, $s_2^* = -\lambda_2^* \cos^2 \theta_2$ as well as the rate of total stretching, $s^* = s_1^* + s_2^*$. For $Ka_0 = 4$, direction \mathbf{x}_1 merely undergoes the action of lowest strain (Fig. 5), and the latter is mostly negative (Fig. 3), which leads to positive stretching throughout the c -range except in the center region where it shows a slightly negative minimum. Conversely, for the lowest Karlovitz

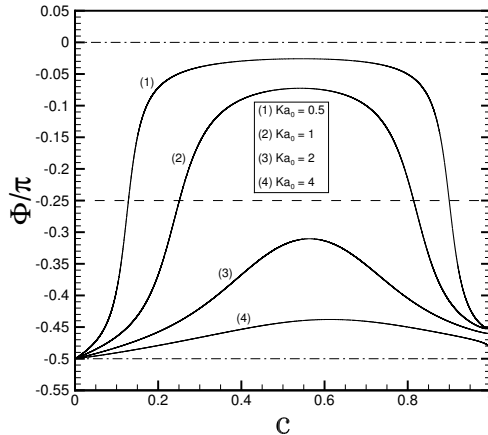


Fig. 5 Angle between direction of highest strain and direction of forcing *vs.* progress variable, c , for Karlovitz number $Ka_0 = 0.5, 1, 2,$ and 4 . The lower the Karlovitz number, the better the alignment of highest strain with the direction of forcing

number, $Ka_0 = 0.5$, alignment is with the highest, positive strain (Fig. 5) and total stretching is essentially negative. Plots for $Ka_0 = 4$ and $Ka_0 = 2$ show intermediate states which are clearly explained by the evolution of strain axes orientation and sign of lowest strain. Again, those findings are akin to recent DNS flame data [14].

The evolution of strain orientation at the crossing of the expansion zone is explained by rotation of strain axes. In this two-dimensional Euler flow, the latter is merely promoted by anisotropy of the pressure Hessian tensor [21]. The rotation rate of strain eigenvectors is expressed by $\Omega = 2D\Phi/Dt = \sigma^{-2}(\sigma_s D\sigma_n/Dt - \sigma_n D\sigma_s/Dt)$, and thus, from Eqs. (2) and (3):

$$\Omega = \sigma^{-2} [\sigma_s (\Pi_{22} - \Pi_{11}) + \sigma_n (\Pi_{12} + \Pi_{21})]. \quad (15)$$

It was checked that varying the Karlovitz number does not significantly change the *intrinsic* anisotropy of pressure Hessian – as measured, for instance, by the anisotropy tensor. Anisotropy measured against strain intensity, by contrast, is highly sensitive to Karlovitz number, as shown in Fig. 8. The latter shows components a_{22} and a_{12} of tensor \mathbf{a} , defined as: $a_{ij} = (2\Pi_{ij} - \Pi_{\alpha\alpha}\delta_{ij})/\sigma^2$, that is, $a_{22} = (\Pi_{22} - \Pi_{11})/\sigma^2$, and $a_{12} = 2\Pi_{12}/\sigma^2$ – in this problem, $\Pi_{12} = \Pi_{21}$. They indicate greater anisotropy of diagonal than non-diagonal components, which is explained by forcing of Π_{11} [Eq. (9)]. Above all, they definitely show the sharp rise of anisotropy as the Karlovitz number is decreased from $Ka_0 = 4$ to $Ka_0 = 0.5$; a_{22} peaks at levels a hundred times higher in the latter case.

As a result, decreasing the Karlovitz number promotes rotation of strain axes. This is clear in Fig. 9 showing the rotation rate, $\Omega^* = Ka_0\Omega$, as well as contributions of anisotropic terms to rotation namely, $a_{22}\sigma_s^*$, and $a_{12}\sigma_n^*$ [Eq. (15)], where $\sigma_s^* = Ka_0\sigma_s$, and $\sigma_n^* = Ka_0\sigma_n$. The other feature is the major contribution of

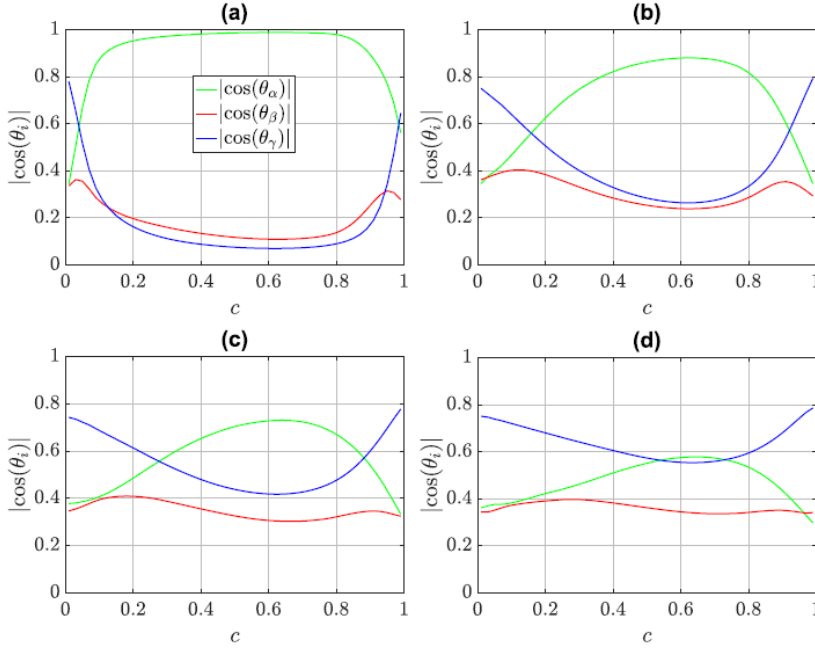


Fig. 6 Mean values of the magnitudes of cosines between strain principal axes and direction normal to the flame, $|\cos(\theta_\alpha)|$, $|\cos(\theta_\beta)|$, and $|\cos(\theta_\gamma)|$, conditioned upon c for heat release parameter 4.5 and Karlovitz number 0.58 (a), 3 (b), 6.5 (c), and 11.9 (d) [14]. The evolution of angle between highest strain and direction of forcing predicted by the model (Fig. 5) is to be compared with the evolution of $|\cos(\theta_\alpha)|$ (green line). Reproduced from “Principal strain rate evolution within turbulent premixed flames for different combustion regimes” by Kasten, C., Ahmed, U., Klein, M., Chakraborty, N., *Physics of Fluids* **33**, 015111 (2021) with permission of AIP Publishing

diagonal anisotropy to strain axes rotation through $a_{22}\sigma_s^*$, at least from low to moderate Karlovitz number. For $Ka_0 = 4$, contribution from $a_{12}\sigma_n^*$ matters.

Finally, the forcing term $\delta^{*2}/2 + D\delta^*/Dt = Ka_0^2(\delta^2/2 + D\delta/Dt)$ – which does not depend on Ka_0 – as well as the pressure Hessian diagonal anisotropic term, $\Pi_{22}^* - \Pi_{11}^* = Ka_0^2(\Pi_{22} - \Pi_{11})$, are plotted in Fig. 10 for $Ka_0 = 0.5, 1, 2$, and 4. At low Karlovitz number, anisotropy of pressure Hessian mostly results from forcing and thus $\Pi_{22} - \Pi_{11} \simeq \delta^2/2 + D\delta/Dt$, which – since, as was checked, $|\Pi_{11}| \gg |\Pi_{22}|$ no matter the Karlovitz number – further gives:

$$\Pi_{11} \simeq -\delta^2/2 - D\delta/Dt, \quad (16)$$

showing that Π_{11} , then, scales as Ka_0^{-2} . And the approximate rotation rate of strain principal axes at low Karlovitz number is:

$$\Omega \simeq \sigma_s(\delta^2/2 + D\delta/Dt)/\sigma^2, \quad (17)$$

which suggests that the shear component of strain is needed in addition to forcing by expansion to trigger strain axes rotation. As mentioned above (Section 2), the shear component itself results from interaction of vorticity with the diagonal

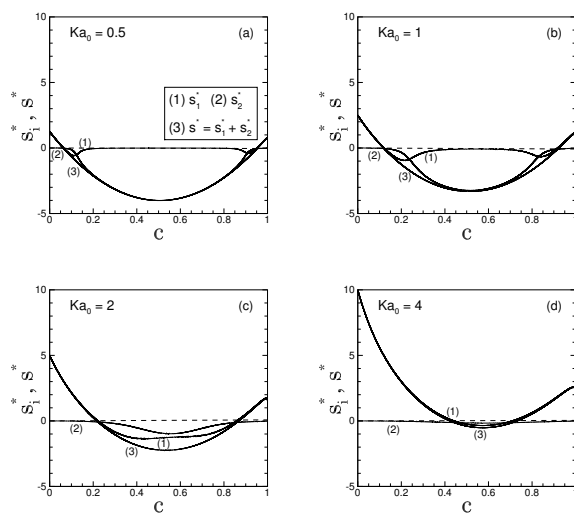


Fig. 7 Rates of stretching parallel to x_1 , s_1^* , and $s^* = s_1^* + s_2^*$, vs. progress variable, c , for Karlovitz number $Ka_0 = 0.5, 1, 2$, and 4 . For large Karlovitz number, total stretching along the direction of forcing is mostly positive, while it is mostly negative for low Karlovitz number

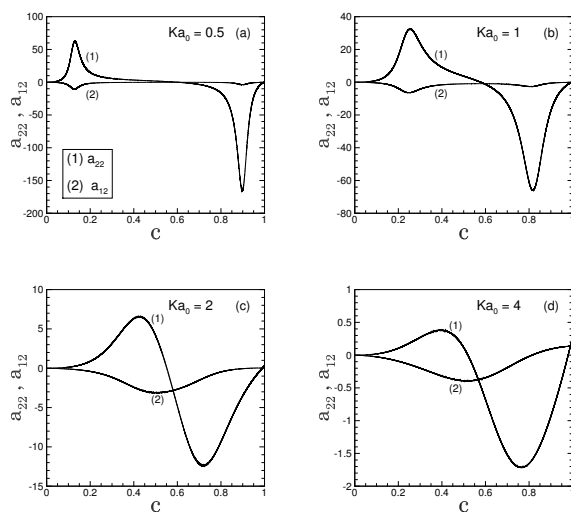


Fig. 8 Components a_{22} and a_{12} of anisotropy tensor of pressure Hessian vs. progress variable, c , for Karlovitz number $Ka_0 = 0.5, 1, 2$, and 4 . The anisotropy of pressure Hessian tensor measured against strain intensity strongly increases with decreasing Karlovitz number

components of pressure Hessian. The present work confirms the key role of the

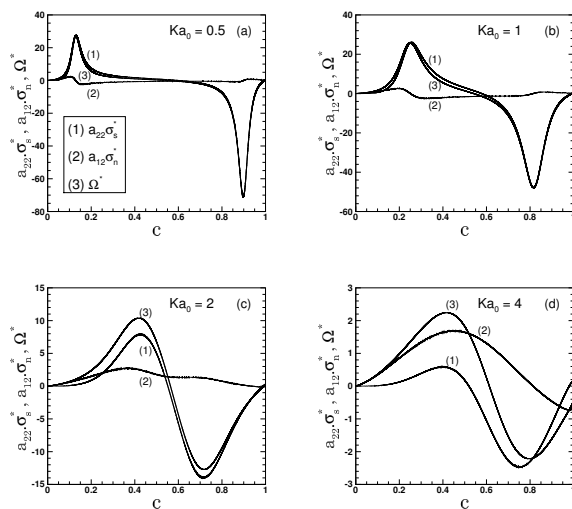


Fig. 9 Rotation rate of strain principal axes, Ω^* , and contributions to rotation, $a_{22}\sigma_s^*$ and $a_{12}\sigma_n^*$, vs. progress variable, c , for Karlovitz number $Ka_0 = 0.5, 1, 2, \text{ and } 4$. Decreasing the Karlovitz number promotes rotation of strain principal axes

pressure Hessian tensor in premixed flames that was surmised from earlier studies [18,22], and recently especially scrutinized [8,15].

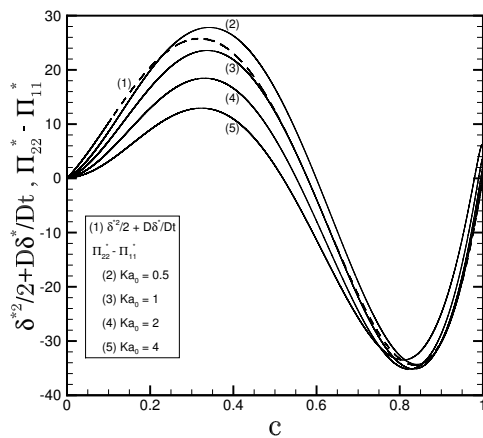


Fig. 10 Forcing term, $\delta^{*2}/2 + D\delta^*/Dt$, and pressure Hessian anisotropic term $\Pi_{22}^* - \Pi_{11}^*$, vs. progress variable, c , for Karlovitz number $Ka_0 = 0.5, 1, 2, \text{ and } 4$. Anisotropy of pressure Hessian tensor essentially results from forcing

3.2 Influence of initial vorticity

3.2.1 Zero initial vorticity

The case of zero initial vorticity is a special one. Keeping the other initial conditions of the above reference test case, $\omega(0) = 0$ indeed leads to $\omega(t) = 0$, $\sigma_s(t) = 0$, and $\sigma(t) = |\sigma_n(t)|$, and to a weak influence of the Karlovitz number, at least within the present range of values.

No matter the value of Ka_0 , the reciprocal local Karlovitz number, δ/σ , is mostly greater than one, and is singular where $\sigma = 0$ as σ_n changes sign. Swapping in σ_n sign also makes the angle between highest strain and direction of forcing, x_1 , switch from $-\pi/2$ to 0, and conversely. Highest strain mostly acts along the direction of forcing – and stretching parallel to x_1 is essentially negative –, except at the ends of c -range.

3.2.2 Low initial vorticity

The latter limit behavior is reflected by the results for low initial vorticity namely, $\omega(0) = 0.05\sigma(0)$. The reciprocal local Karlovitz number and the angle between highest strain and direction x_1 are plotted in Fig. 11. The latter is to be compared to Figs. 2 and 5. Plots in Fig. 11 shows that $\delta/\sigma > 1$ right from the lowest c values up to the higher end of c -range, which implies expansion prevailing over flow strain and positive lowest strain, λ_1 , there. Direction of highest strain is mostly parallel to x_1 . And the weak dependence on the Karlovitz number is striking.

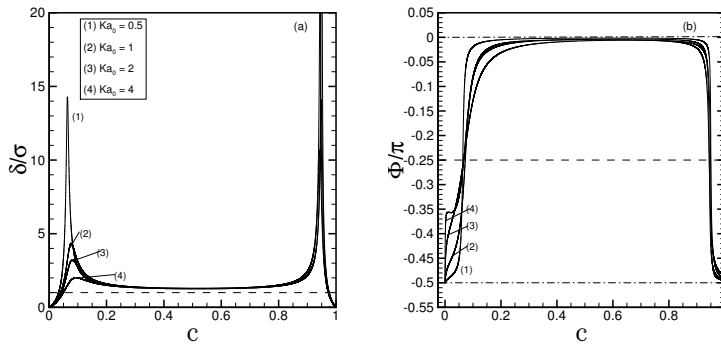


Fig. 11 (a) Reciprocal of local Karlovitz number, and (b) angle between direction of highest strain and direction of forcing, *vs.* progress variable, c , for $\omega(0) = 0.05\sigma(0)$ and Karlovitz number $Ka_0 = 0.5, 1, 2,$ and 4 ; peaks of δ/σ around $c \simeq 0.95$ are clipped at $\delta/\sigma = 20$. For low initial vorticity, expansion merely prevails over flow strain, and direction of highest strain is mostly parallel to the direction of forcing

3.3 Influence of initial strain

The effect of initial strain was checked for $\sigma_n(0) = -0.5Ka_0\delta_m$, and $\sigma_n(0) = -2Ka_0\delta_m$ while keeping the conditions of the reference test case for other variables, namely $c(0) = 10^{-4}$, $\sigma_s(0) = 0$, $\omega(0) = \sigma(0)$, and isotropy of pressure Hessian.

Plainly, increasing the initial strain – i.e. strain of incident flow, if any analogy with a flame problem is made – lessens expansion effects. Figure 12 – as well as comparison with Fig. 2 for $\sigma_n(0) = -Ka_0\delta_m$ – shows that the lower $\sigma_n(0)$, the wider the c -range over which δ/σ exceeds unity. For $\sigma_n(0) = -2Ka_0\delta_m$, mitigation of expansion effect is enough to keep δ/σ below one for $Ka_0 = 4$, which implies one compressional and one extensional strain direction throughout the c -range.

Plots for Φ show similar trends (Fig. 13). The lower the initial strain, the better the alignment of the highest strain with x_1 . But increasing $\sigma_n(0)$ prevents this alignment; it is the lowest strain that aligns with x_1 for $Ka_0 = 1, 2$, and 4, if $\sigma_n(0) = -2Ka_0\delta_m$.

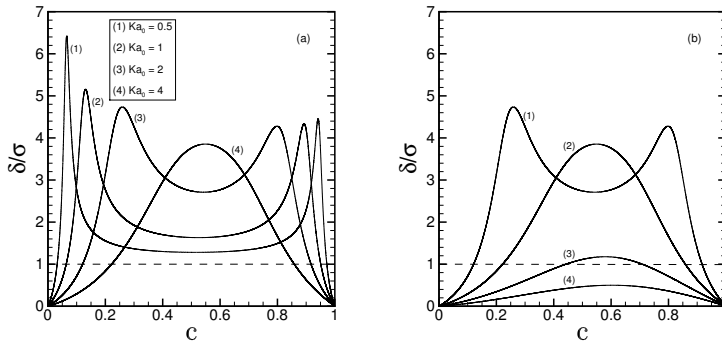


Fig. 12 Reciprocal of local Karlovitz number *vs.* progress variable, c , for (a) $\sigma_n(0) = -0.5Ka_0\delta_m$, and (b) $\sigma_n(0) = -2Ka_0\delta_m$; Karlovitz number $Ka_0 = 0.5, 1, 2$, and 4. Increasing initial strain lessens expansion effects

4 Conclusion

The principle of the model problem developed in this study is twofold. First, the expansion rate at the crossing of a premixed flame front is mimicked by specifying a likely evolution in function of a progress variable. And second, the forcing resulting from expansion is explicitly included in the computation of one diagonal component of the pressure Hessian. This defines a special direction – referred to as the direction of forcing – that can stand for the normal to a flame front, and along which anisotropy of the pressure Hessian is triggered by expansion. Running the model consists in solving the evolution equations for the progress variable, the normal and shear components of strain, vorticity, and three components of the pressure Hessian. The model includes two independent parameters, namely the

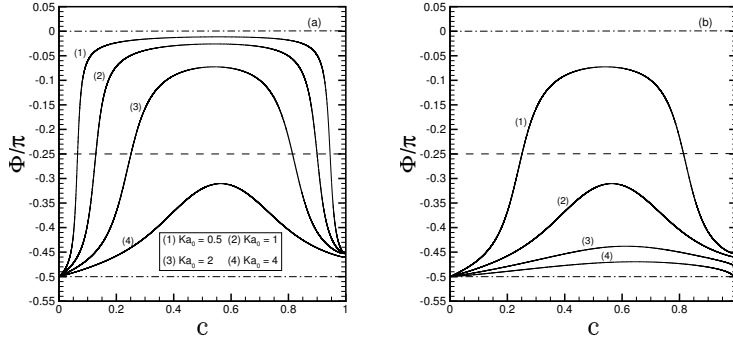


Fig. 13 Angle between direction of highest strain and direction of forcing, *vs.* progress variable, c , for (a) $\sigma_n(0) = -0.5Ka_0\delta_m$, and (b) $\sigma_n(0) = -2Ka_0\delta_m$; Karlovitz number $Ka_0 = 0.5, 1, 2, \text{ and } 4$. The lower the initial strain, the better the alignment of highest strain with the direction of forcing

heat release parameter and a Karlovitz number defined as the ratio of strain rate to expansion rate. The analysis addressed the influence of the Karlovitz number on strain evolution.

Apart from features specific to the two-dimensional case – such as more likely positive lowest strain –, the model results are akin to the evolution of strain approaching a flame front as reported in recent studies. This is true, in particular, for strain eigenvalues, rate of stretching in the direction of forcing, and orientation of strain principal axes, when varying the Karlovitz number. Low Karlovitz number indeed promotes alignment of highest strain with the direction of forcing – and negative stretching in this direction –, while increasing the Karlovitz number leads to alignment of lowest strain with direction of forcing, and positive stretching. Those findings thus suggest that the model includes basic mechanisms of the physics of the velocity gradient in flame fronts, and moreover, that mass density changes due to heat release may indeed be enough to explain the overall behavior of strain at the crossing of a flame front.

In this regard, the model shows that the special evolution of strain axes rotation which, at low Karlovitz number, at first brings the direction of highest strain close to the direction of forcing and then reverses, leading to alignment of lowest strain with forcing, is reminiscent of recent simulation data on alignment of strain with the normal to a flame front. Furthermore, it suggests that this behavior is mainly caused by anisotropy of pressure Hessian resulting from forcing by expansion. The model thereby confirms the essential role of pressure Hessian in strain physics in flames that had been pointed out in earlier works, and recently ascertained by numerical simulations. Addressing the three-dimensional problem would give further insight into this physics.

Data Availability Statement – The datasets generated during and/or analysed during the current study are available from the corresponding author on reasonable request.

Acknowledgements The author acknowledges permission of AIP and of Professor Nilanjan Chakraborty to use two figures of reference [14].

References

1. Danish, M., Suman, S., Girimaji, S.S.: Influence of flow topology and dilatation on scalar mixing in compressible turbulence. *J. Fluid Mech.* **793**, 633-655 (2016)
2. Boukharfane, R., Bouali, Z., Mura, A.: Evolution of scalar and velocity dynamics in planar shock-turbulence interaction. *Shock Waves* **28**, 1117-1141 (2018)
3. Boratav, O.N., Elghobashi, S.E., Zhong, R.: On the alignment of strain, vorticity and scalar gradient in turbulent, buoyant, nonpremixed flames. *Phys. Fluids* **10**, 2260-2267 (1998)
4. Swaminathan, N., Grout, R.W.: Interaction of turbulence and scalar fields in premixed flames. *Phys. Fluids* **18**, 045102 (2006)
5. Chakraborty, N., Rogerson, J.W., Swaminathan, N.: The scalar gradient alignment statistics of flame kernels and its modelling implications for turbulent premixed combustion. *Flow Turbulence Combust.* **85**, 25-55 (2010)
6. Hamlington, P.E., Poludnenko, A.Y., Oran, E.S.: Interactions between turbulence and flames in premixed reacting flows. *Phys. Fluids* **23**, 125111 (2011)
7. Dopazo, C., Cifuentes, L.: The physics of scalar gradients in turbulent premixed combustion and its relevance to modeling. *Combust. Sci. and Tech.* **188**, 1376-1397 (2016)
8. Zhao, S., Er-ray, A., Bouali, Z., Mura, A.: Dynamics and kinematics of the reactive scalar gradient in weakly turbulent premixed flames. *Combust. Flame* **198**, 436-454 (2018)
9. Zhao, S., Mura, A.: Turbulence topology evolution in weakly turbulent premixed flames. *Phys. Fluids* **33**, 035110 (2021)
10. Chakraborty, N., Swaminathan, N.: Influence of the Damköhler number on turbulence-scalar interaction in premixed flames. I. Physical insight. *Phys. Fluids* **19**, 045103 (2007)
11. Mura, A., Tsuboi, K., Hasegawa, T.: Modelling of the correlation between velocity and reactive scalar gradients in turbulent premixed flames based on DNS data. *Combust. Theory Modell.* **12**, 671-698 (2008)
12. Dopazo, C., Cifuentes, L., Martin, J., Jimenez, C.: Strain rates normal to approaching iso-scalar surfaces in a turbulent premixed flame. *Combust. Flame* **162**, 1729-1736 (2015)
13. Steinberg, A.M., Coriton, B., Frank, J.H. Influence of combustion on principal strain-rate transport in turbulent premixed flames. *Proc. Combust. Inst.* **35**, 1287-1294 (2015)
14. Kasten, C., Ahmed, U., Klein, M., Chakraborty, N.: Principal strain rate evolution within turbulent premixed flames for different combustion regimes. *Phys. Fluids* **33**, 015111 (2021)
15. Gonzalez, M.: Analyzing the effect of dilatation on the velocity gradient tensor using a model problem. *SN Applied Sciences* **2**, 1793-1797 (2020)
16. Suman, S., Girimaji, S.S.: Dynamical model for velocity-gradient evolution in compressible turbulence. *J. Fluid Mech.* **683**, 289-319 (2011)
17. Tien, J.H., Matalon, M.: On the burning velocity of stretched flames. *Combust. Flame* **84**, 238-248 (1991)
18. Gonzalez, M., Paranthoën, P.: Effect of variable mass density on the kinematics of the scalar gradient. *Phys. Fluids* **23**, 075107 (2011)
19. Nomura, K., Elghobashi, S.: The structure of inhomogeneous turbulence in variable density nonpremixed flames. *Theor. Comput. Fluid Dyn.* **5**, 153-175 (1993)
20. Steinberg, A.M., Driscoll, J.F., Swaminathan, N.: Statistics and dynamics of turbulence-flame alignment in premixed combustion. *Combust. Flame* **159**, 2576-2588 (2012)
21. Lapeyre, G., Klein, P., Hua, B.L.: Does the tracer gradient align with strain eigenvectors in 2D turbulence? *Phys. Fluids* **11**, 3729-3737 (1999)
22. Gonzalez, M., Paranthoën, P.: Effect of density step on stirring properties of a strain flow. *Fluid Dyn. Res.* **41**, 035508 (2009)